A fast control for a three-switch multi-input DC-DC converter

Simone Cosso, Andrea Formentini, Mario Marchesoni, Massimiliano Passalacqua, Luis Vaccaro

UNIVERSITY OF GENOVA, DEPARTMENT OF ELECTRICAL, ELECTRONIC, TELECOMMUNICATIONS ENGINEERING AND NAVAL ARCHITECTURE
Via all' Opera Pia 11A,16145
Genova, Italy
simone.cosso@edu.unige.it, andrea.formentini@unige.it, marchesoni@unige.it, massimiliano.passalacqua@unige.it, luis.vaccaro@unige.it

Keywords: «DC-DC Converter» «Feed-Forward» «DCM» «CCM» «Power Converters»

Abstract
In this paper, a double-input bidirectional DC-DC converter is taken into account. The converter allows to use less switches than a traditional solution and, moreover, it guarantees a higher efficiency. The modulation strategy proposed in the technical literature allows the converter to work in Discontinuous Conduction Mode at low-load and, therefore, to increase the efficiency in comparison to the CCM. However, such a control reduces the dynamics of the converter. To improve the transient response, a Feed-Forward approach is proposed in this paper. Since the converter model in DCM is complex and highly nonlinear, a simplified model is considered. The effectiveness of the proposed approach is proved with experimental results on a converter prototype.

Introduction
The increasing attention on air pollution and greenhouse emissions led to increasing attention on renewable energy sources and in electric mobility. Regarding the power electronics sector, this aspect increases the studies on DC-DC converters. As a matter of fact, DC-DC converters are used to interface renewables and storages with a common DC-bus [1-4]; moreover, the storage systems are connected with DC-DC converters with the motor inverter DC-link in hybrid and electric vehicles [5-9]. When several DC sources are used, it could be useful to use multi-input or multi-output converters. Various solutions are proposed in the technical literature both with galvanic insulation [10-14] and without galvanic insulation [15-19].
Regarding bidirectional multi-input single-output converters, a new double-input converter is shown in [20]. The proposed converter uses only three switches, whereas in a conventional solution (i.e., two half-bridge converters in parallel connection) four switches are needed. Moreover, the converter proposed in [20] guarantees lower losses in comparison to two half-bridges converters, as shown in [20] and analyzed in detail in [21]. However, in low-load working conditions, the converter works in Continuous Conduction Mode (CCM) with the control strategy proposed in [20].
To improve the efficiency in this working region by exploiting Discontinuous Conduction Mode (DCM), a new modulation strategy is presented in [22]. Moreover, in [20] the current path at high loads is also optimized and a loss reduction is achieved also in this working area.
However, the efficiency increase is obtained at the cost of dynamics reduction; as a matter of fact, in DCM the converter becomes strongly nonlinear. Indeed, as highlighted in the paper, in CCM a small variation in the control output (i.e., switch duty cycles) causes a high variation in the converter currents, whereas, in DCM a high variation in the control output causes a low variation in the converter currents. For this reason, an optimal control tuning in the CCM region causes a very slow response in the DCM region, whereas an optimal control tuning in the DCM region causes instability in the CCM region. Since the converter is strongly nonlinear in the DCM region, also the CCM-DCM bound depends on several variables and, therefore, variable gains lead analogously to instability.
In this paper, a Feed-Forward (FF) control is proposed to improve the converter speed response. A simplified converter model is studied and it is used to calculate the duty cycle values for the desired current references. The proposed control is integrated into the control proposed in [20]. The effectiveness of this solution is verified with experimental tests on a converter prototype.

Converter structure and control

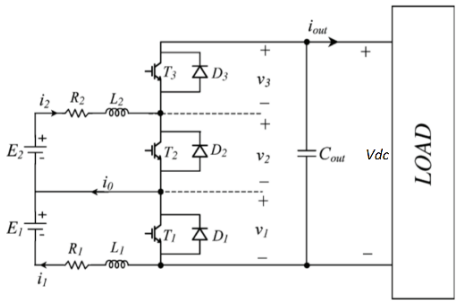

Fig. 1. Three-switch double-input bidirectional DC-DC converter.

The three-switch converter is shown in Fig. 1. The converter is a double-input bidirectional boost, i.e., the sum of the two-input voltages E_1 and E_2 has to be lower than the output voltage Vdc.
In Fig. 2 the control developed in [22] is shown. In order to allow DCM at low loads, five different working conditions are identified. Control outputs, gains K_1 and K_2 varies according to the working condition as shown in Fig. 2.
Please note that i_1 and i_2 are the current instantaneous values whereas I_1 and I_2 are the current average values during the duty cycle. The five working conditions depends on current reference and are listed in the followings:

1. $I_1 > 0, I_2 > 0$
2. $I_1 > 0, I_2 < 0$
3. $I_1 < 0, I_2 > 0$
4. $I_1 < 0, I_2 < 0, I_1 > I_2$
5. $I_1 < 0, I_2 < 0, I_1 < I_2$

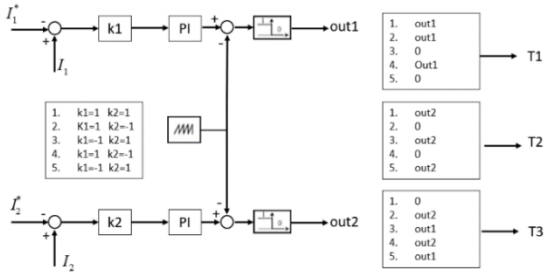

Fig. 2. The control scheme for the three-switch converter.

If both currents are positive and the converter works in CCM, the relation between I_1 and m_1 (i.e., the duty cycle of switch 1), and I_2 and m_2 can be modelled by the transfer functions in equations (1):

$$\frac{I_1}{m_1} = \frac{V_{dc}}{(R_1 + sL_1)(sT_p + 1)}; \quad \frac{I_2}{m_2} = \frac{V_{dc}}{(R_2 + sL_2)(sT_p + 1)} \qquad (1)$$

Where V_{dc}, R_1, R_2, L_1 and L_2 are shown in Fig. 1, whereas T_p is the converter delay, which can be considered 1.5 the switching frequency.
The control PI gains can be tuned from equations (1) (e.g., using the phase margin criterion). Even if a fast response is obtained in CCM, the converter dynamics worsens significantly in DCM. Indeed, the tuning in CCM (i.e., starting from equations (1)) leads to PI gains which are too low for the DCM region.
In order to fasten the response, a FF approach is carried out in this paper.

The feed-forward inputs guarantee a fast response, with a small error, which is then annulled by the PI with a time constant that can be relatively high. For the sake of brevity, the FF equations are shown just for condition 1. However, the same method can be applied also to the other four conditions. Please note that in the test bench control platform the FF control is implemented for all the five conditions in order to perform the experimental tests.

Feed-Forward approach

Fig. 3 shows the four possible current paths in condition 1 (i.e., when both I_1 and I_2 are positive). For each path, one can calculate the current slopes (i.e., the current derivatives), which depends on the voltage and inductance values. The current slopes for each path are reported in Table I, together with the related switch configuration.

In the low-load region, the transfer function between the switch duty cycles and the currents vary according to several variables (e.g., the current signs, the current amplitude and based on which current is higher). In addition to that, in path D the transfer function becomes very complex to calculate and difficult to implement in the control.

For this reason, a simplified approach is considered in this study and the relation between duty cycles and current references are approximated with an heuristic approach.

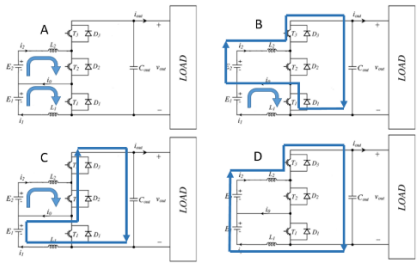

Fig. 3. Current paths in condition 1 (I_1 and I_2 >0)

TABLE I. CURRENT SLOPES AND IGBT CONFIGURATION IN CONDITION 1

Path	IGBT config.	Current slope I1	Current slope I2
A	T_1 on T_2 on T_3 off	$\frac{V_1}{L_1}$	$\frac{V_2}{L_1}$
B	T_1 on (or T_1 off and $i_1<i_2$) T_2 off T_3 off	$\frac{V_1}{L_1}$	$\frac{V_{dc}-V_2}{L_2}$
C	T_1 off T_2 on (or T_2 off and $i_2<i_1$) T_3 off	$\frac{V_{dc}-V_2}{L_1}$	$\frac{V_2}{L_1}$
D	T_1 off T_2 off T_3 off	$\frac{V_{dc}-V_1-V_2}{L_1+L_2}$	$\frac{V_{dc}-V_1-V_2}{L_1+L_2}$

The instantaneous current waveforms in condition 1 are shown in Fig. 4. It is possible to note that when all switches are off, path C occurs at first; then, when I_1 and I_2 reach the same instantaneous value, the two currents decrease overlapping (i.e., path D occurs).

During path D, current slope is $\frac{V_{dc}-V_1-V_2}{L_1+L_2}$, whereas it is $\frac{V_{dc}-V_2}{L_2}$ and $\frac{V_{dc}-V_1}{L_1}$ in path B and C, respectively. Differently, when both switches T1 and T2 are closed, current path A occurs and both currents increase independently.

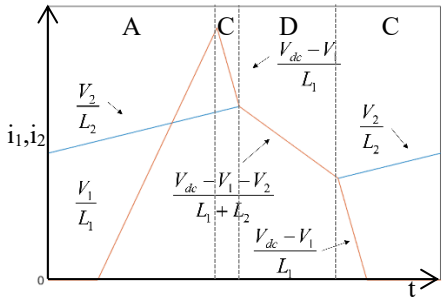

Fig. 4. Condition 1, $I_1>0$ and $I_2>0$ waveforms. i_1 (red), i_2 (blue).

From Fig. 4 one can note that the mathematical relation between the duty cycles and the current references is hard to obtain and unsuitable to implement in the control. For this reason a simplified method is proposed in the followings.
The relation between duty cycles and currents is evaluated in the two limit conditions: when there is no overlap (NOV) and when there is a total overlap (TOV), i.e., when $I_1=I_2$. Once this two conditions are evaluated, one can obtain the FF duty cycle values in case of partial overlap, interpolating the NOV and TOP values. As it is shown later, a parameter K to define the overlap ratio is defined.
In the simplified model, six different conditions can be considered:

1) $I_1 < I_2, I_1 > 0, I_2 > 0$ (NOV and TOV)
2) $I_1 < I_2, I_1 < 0, I_2 > \hat{I}_2$ (NOV)
3) $I_1 < I_2, I_1 < 0, I_2 < \hat{I}_2$ (NOV and TOV)
4) $I_1 > I_2, I_1 > 0, I_2 > 0$ (NOV and TOV)
5) $I_1 > I_2, I_1 > \hat{I}_1, I_2 > 0$ (NOV)
6) $I_1 > I_2, I_1 < \hat{I}_1, I_2 < 0$ (NOV and TOV)

$\hat{I}_1$ and $\hat{I}_2$ are defined later in the paper and they are always positive quantities. For this reason, in the 2nd and the 5th conditions the currents have opposite signs, therefore the overlap is not possible. Please note that these are the six conditions to define the FF and should not be confused with the five conditions used to implement the control shown in the previous paragraph.

Feed-forward equations for condition 1

NOV, equation for m2

In Fig. 5 (left) the ideal DCM waveform for i_2 in condition 1 ($I_1 > 0$ and $I_2 > 0$) is shown. Please note that if both currents are in DCM, path D always occur and the real current waveforms are shown in Fig. 5 (right). However, considering the ideal case is useful to obtain the equation to use in the interpolation process.

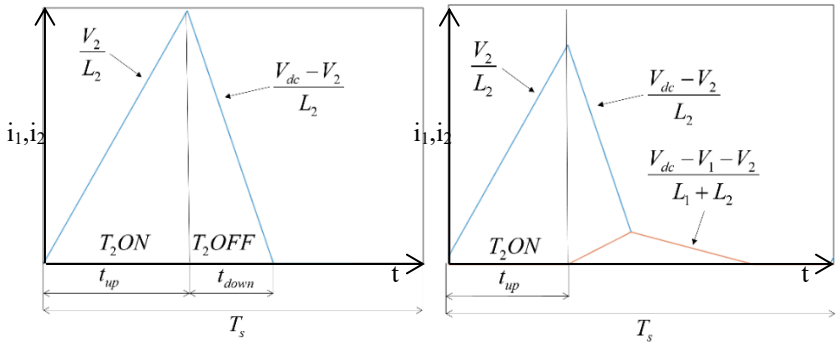

Fig. 5. Ideal waveform of i_2 (left), real waveform of i_2 (right)

The quantities t_{up}, I_{peak} and t_{down} are defined in equations (2), (3) and (4) and the calculation of the average current I_2 is evaluated in equation (5). From equations (2), (3), (4), (5) one can obtain equation (6), which is valid if i_2 is in DCM.

$$t_{up} = m_2 \cdot Ts \tag{2}$$

$$I_{peak} = \frac{V_2}{L_2} \cdot t_{up} \tag{3}$$

$$t_{down} = \frac{I_{peak}}{\frac{V_{dc}-V_2}{L_2}} \tag{4}$$

$$I_2 = \frac{I_{peak} \cdot (t_{up} + t_{down})}{2 \cdot T_s} \tag{5}$$

$$m_2 = \sqrt{\frac{2L_2(V_{dc}-V_2)}{V_2 T_s V_{dc}}} \sqrt{I_2} \tag{6}$$

When i_2 is in CCM, equation (7) is verified. Replacing (6) in (7) one obtains the condition in equation (8), which is valid for the CCM zone, whatever I_2 amplitude. Thus, in case of NOV when both current are positive and $I_1<I_2$ (ideal case), the FF contribution for m_2 is given by equation (6), with the condition that $m_2 \in \left[0; \frac{V_{dc}-V_2}{V_{dc}}\right]$.

$$\frac{V_2}{L_2} m_2 = \frac{V_{dc}-V_2}{L_2}(1-m_2) \tag{7}$$

$$m_2 = \frac{V_{dc}-V_2}{V_{dc}} \tag{8}$$

NOV, $I_1 > \hat{I}_1$, equation for m_1

In Fig. 6, i_1 waveform (red) is plotted together with i_2 waveform (blue). The quantities t_{up}, I_{peak} and t_{down} are defined in equations (9), (10), (11) and the calculation of the average current I_2 is evaluated in equation (12). Please note that in order to simplify the notation, avoiding long subscripts, the definition of t_{up}, I_{peak} and t_{down} is valid until the end of the subparagraph and the same variable are redefined in each subparagraph.

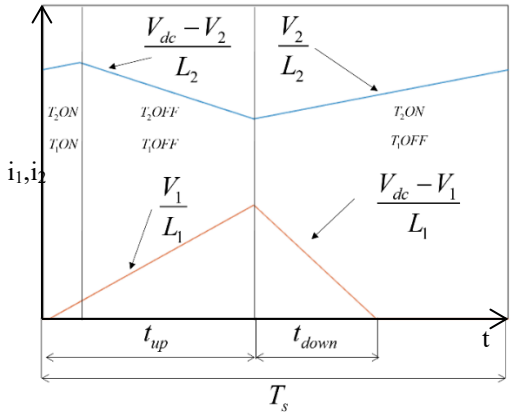

Fig. 6. i_1(red) and i_2(blue) waveforms during a switching period.

$$t_{up} = (m_1 + 1 - m_2)T_s \tag{9}$$

$$I_{1peak} = \frac{V_1}{L_1} t_{up} \tag{10}$$

$$t_{down} = \frac{I_{1peak}}{\frac{(V_{dc} - V_1)}{L_1}} \tag{11}$$

$$I_1 = \frac{I_{1peak}(t_{up} + t_{down})}{2T_s} \tag{12}$$

$$m_1 = \sqrt{\frac{2L_1(V_{dc} - V_1)}{T_s V_1 V_{dc}}}\sqrt{I_1} + m_2 - 1 \tag{13}$$

When i_2 is in CCM, equation (14) is verified. Replacing (13) in (14), (15) is obtained, which is valid for the CCM zone, whatever I_2 amplitude. Thus, in case of NOV, when both currents are positive and $I_1<I_2$, the FF contribution for m_1 is given by equation (15), with the condition that $m_1 = \frac{V_{dc} - V_1}{V_{dc}}$.

$$\frac{V_1}{L_1}(m_1 - m_2 + 1) = \frac{(V_{dc} - V_1)}{L_1}(m_2 - m_1) \tag{14}$$

$$m_1 = \frac{V_{dc} - V_1}{V_{dc}} \tag{15}$$

Please note that when m_1 is zero, I_1 is higher than zero, as it can be noticed in Fig. 7. $\hat{I}_1$ is I_1 value when m_1=0. $\hat{I}_{1NOV}$ is I_1 value while m_1=0 and there is no overlap, i.e., i_2 is in CCM. Substituting m_1=0 and $m_2 = \frac{V_{dc} - V_2}{V_{dc}}$ in equation (13) one obtains equation (16). Since I_1 tends to zero while I_2 tends to zero, $\hat{I}_{1TOV} = 0$. Therefore, the FF value is given by the interpolation between $\hat{I}_{1NOV}$ and $\hat{I}_{1TOV}$.

$$\hat{I}_{1NOV} = \frac{T_s V_1 V_2^2}{2L_1 \mathrm{V}_{dc}(V_{dc} - V_1)} \tag{16}$$

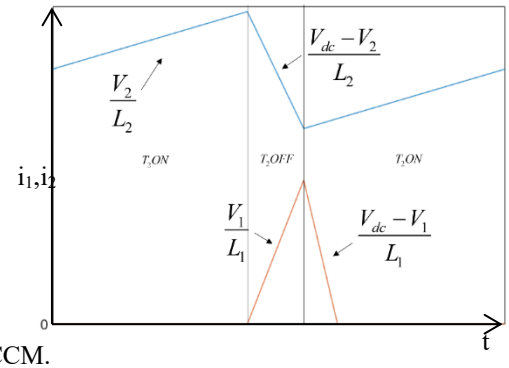

Fig. 7. i_1(red) in DCM and i_2(blue) in CCM.

NOV, $I_1 < \hat{I}_1$, equation for m_1

In Fig. 8, the current waveforms when $I_1 < \hat{I}_1$ and there is NOV are shown. Please note that in this condition, I_1 is controlled by m_3. t_1, $i_{1peakNeg}$, t_2, t_3, $I_{1peakPos}$ and t_4 are defined in equation (17), (18), (19), (20), (21) and (22), whereas the calculation of the I_1 is shown in equation (23).

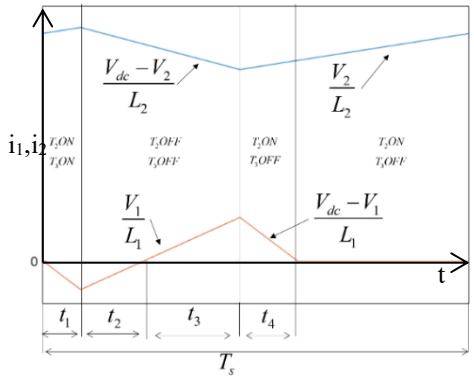

Fig. 8. i_1(red) and i_2(blue) in $I_1 < \hat{I}_1$ condition.

$$t_1 = m_3 T_s \tag{17}$$

$$I_{1peakNeg} = t_1 \frac{V_{dc} - V_1}{L_1} \tag{18}$$

$$t_2 = \frac{I_{1peakNeg}}{\frac{V_1}{L_1}} \tag{19}$$

$$t_3 = 1 - m_2 - t_2 \tag{20}$$

$$I_{1peakPos} = \frac{V_1}{L_1} t_3 \tag{21}$$

$$t_4 = \frac{I_{1peakPos}}{\frac{V_{dc} - V_1}{L_1}} \tag{22}$$

$$I_1 = \frac{I_{1peakPos}(t_3 + t_4) - I_{1peakNeg}(t_1 + t_2)}{2T_s} \tag{23}$$

Substituting (17), (18), (19), (20), (21) and (22) in (23), one obtains (24).

$$m_3 = \frac{V_1(1-m_2)}{2(V_{dc}-V_1)} - \frac{L_1}{T_s V_{dc}(1-m_2)} I_1 \tag{24}$$

It is worth to note that equation (24) is valid only when there is NOV, therefore $m_2 = \frac{V_{dc}-V_2}{V_{dc}}$. Substituting m_2 expression in (24) one obtains equation (25).

$$m_3 = \frac{V_1 V_2}{2V_{dc}(V_{dc}-V_1)} - \frac{L_1}{T_s V_2} I_1 \tag{25}$$

TOV, equations for m_1 and m_2

In the previous subparagraphs the condition in which there is not current overlap (NOV) has been shown. Now, the other condition, i.e., when $i_1=i_2$ and there is a total overlap (TOV), is taken into account. The current waveforms in this condition are shown in Fig. 9. Neglecting the small time in which current slopes have opposite signs, one can define t_{2up}, I_{2peak}, t_{2down} and I_2 as in equations (26), (27), (28), and (29).

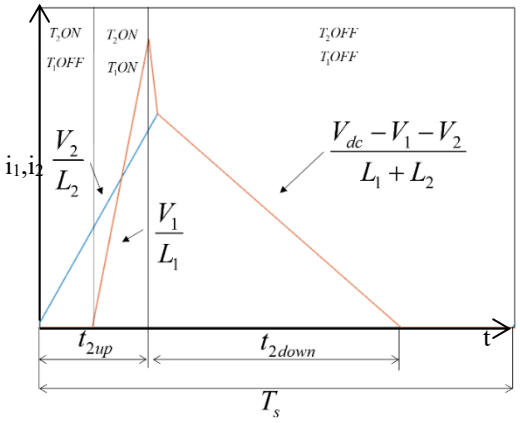

Fig. 9. i_1(red) and i_2(blue) waveform when $I_1=I_2$.

$$t_{2up} = m_2 T_s \tag{26}$$

$$I_{2peak} = \frac{V_2}{L_2} t_{2up} \tag{27}$$

$$t_{2down} = \frac{I_{2peak}}{\frac{V_{dc}-V_1-V_2}{L_1+L_2}} \tag{28}$$

$$I_2 = \frac{I_{2peak}(t_{2up}+t_{2down})}{2T_s} \tag{29}$$

Combining the previous equations, one obtains equation (30).

$$m_2 = \sqrt{\frac{2L_2^2(V_{dc}-V_1-V_2)}{V_2 T_s (L_1 V_2 - L_2 V_1 + L_1 V_{dc})}} \sqrt{I_2} \tag{30}$$

Equation (30) is valid when i_2 is in DCM. On the contrary, equation (31) is verified when i_2 is in CCM. Substituting (26), (27) and (28) in (31) equation (32) is obtained and solving for m_2 results in equation (33). Thus, the FF contribution for m_2 in this condition is given by equation (30) with the limitation $m_2 \in \left[0; \frac{L_2(V_{dc}-V_1-V_2)}{(L_1 V_2 - L_2 V_1 + L_2 V_{dc})}\right]$.

$$t_{2up} = t_{2down} \tag{31}$$

$$\frac{V_2 m_2}{L_2} = \frac{V_{dc} - V_1 - V_2}{L_1 + L2}(1 - m_2) \tag{32}$$

$$m_2 = \frac{L_2(V_{dc} - V_1 - V_2)}{(L_1 V_2 - L_2 V_1 + L_2 V_{dc})} \tag{33}$$

t_{1up} , I_{1peak} , t_{1down} and I_1 are defined in equations (34), (35), (36) and (37). Substituting (34), (35) and (36) in (37) one obtains equation (38).

$$t_{1up} = m_1 T_s \tag{34}$$

$$I_{1peak} = \frac{V_1}{L_1} t_{1up} \tag{35}$$

$$t_{1down} = \frac{I_{1peak}}{\frac{V_{dc} - V_1 - V_2}{L_1 + L_2}} \tag{36}$$

$$I_1 = \frac{I_{1peak}(t_{1up} + t_{1down})}{2T_s} \tag{37}$$

$$m_1 = \sqrt{\frac{2L_1^2}{T_s V_1}\left(\frac{Vdc - V_1 - V_2}{L_2 V_1 - L_1 V_2 + L_1 V_{dc}}\right)}\sqrt{I_1} \tag{38}$$

Since with a TOV i_1=i_2, if $\frac{V_2}{L_2} < \frac{V_1}{L_1}$, then $m_1 \in [0; m_2]$. On the contrary if $\frac{V_2}{L_2} > \frac{V_1}{L_1}$, then $m_1 \in \left[0; \frac{L_1(V_{dc} - V_1 - V_2)}{(L_2 V_1 - L_1 V_2 + L_1 V_{dc})}\right]$ and $m_2 \in [0; m_1]$.

Interpolation Process

The interpolation process is used to find feed-forward outputs while there is a partial overlap. The current ripples when both currents are in CCM and without overlap are defined in equations (39) and (40). If the currents are in DCM and there is no overlap, it is easy to verify that the ripple is given by equations (41) and (42). Therefore, a parameter K, which measures the overlap ratio, is defined in equation (43). Since in equations (6), (13), (30) and (38) the current is under square root, the duty cycles can be calculated as in equation (44).

$$di_1 = \frac{V_1(V_{dc} - V_1)T_s}{L_1 V_{dc}} \tag{39}$$

$$di_2 = \frac{V_2(V_{dc} - V_2)T_s}{L_2 V_{dc}} \tag{40}$$

$$di_{1real} = di_1 \sqrt[(sign)]{\frac{I_1}{di_1 / 2}} \qquad di_{1real} \in [-d_{i1}; d_{i1}] \tag{41}$$

$$di_{2real} = di_2 \sqrt[(sign)]{\frac{I_2}{di_2 / 2}} \qquad di_{2real} \in [-d_{i2}; d_{i2}] \tag{42}$$

$$K = \left|\frac{2(I_2 - I_1)}{|di_{1real} + di_{2real}|}\right| \in [0;1] \tag{43}$$

$$m_x = \sqrt{K} m_{x(NOV)} + (1 - \sqrt{K}) m_{x(TOV)} \tag{44}$$

Experimental results

The proposed FF approach is tested on a converter prototype, which is shown in Fig. 10. A 12V battery and a 22V supercapacitor are employed as sources, whereas there is no load on the DC-link, therefore one source charges the other one. A voltage-loop is implemented to keep the DC-link at 150 V. Therefore I_1 reference is the voltage PI output, whereas I_2 reference can be set arbitrarily. The control is implemented of Dspace Microlabbox.

Currents waveform while I_2 reference is changed from +5V to -5V are shown in Fig. 11, both for the control with and without FF. Moreover, in Fig. 12 a test with a sinusoidal reference for I_2 at 3Hz is shown both with and without FF. Please note that in order to plot the current reference, Fig. 12 is obtained exporting the data from Dspace and post-processing them with Matlab.

In both cases one can note a significant increase in dynamics with the FF control.

Fig. 10 Experimental test bench.

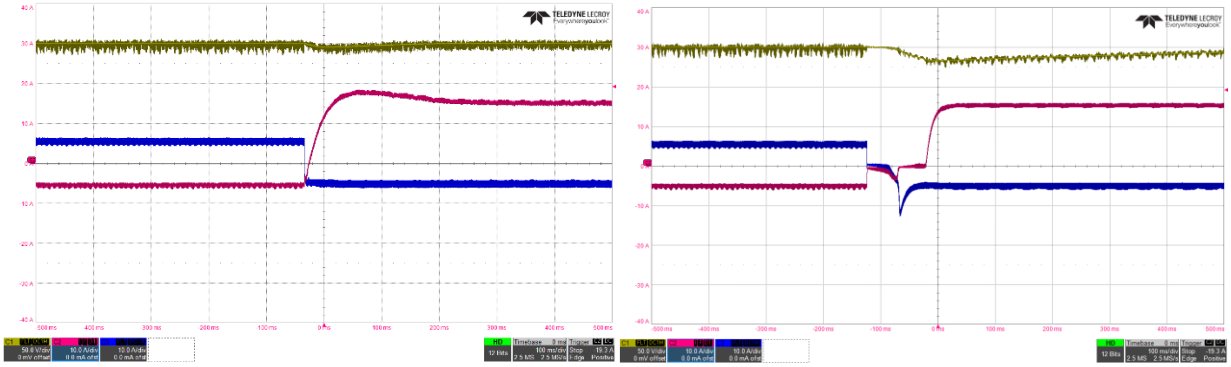

Fig. 11. i_1(magenta), i_2(blue) and v_{dc}(yellow) during a I_2 variation from +5 A to -5A. FF (left), NO-FF (right).

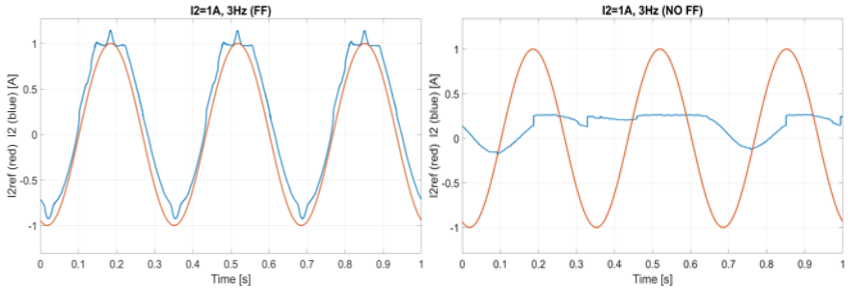

Fig. 12 Experimental current I_2(blue) and reference (red) at 1 A, 3 Hz. FF (left), NO-FF (right).

Conclusions

In this paper a double-input bidirectional DC-DC converter is taken into account. The modulation proposed in the technical literature to work in DCM allows loss reduction, however it worsen the converter dynamics. To improve the transient response, a Feed-Forward control is proposed in this paper and added to the converter control. Since the converter model in DCM is highly nonlinear

and complex, simplified relations are considered for the Feed-Forward. The effectiveness of the proposed strategy is validated with experimental results on a converter prototype comparing the transient response with and without Feed-Forward.

REFERENCES

[1] H. Fakham, D. Lu, and B. Francois, "Power Control Design of a Battery Charger in a Hybrid Active PV Generator for Load-Following Applications," *IEEE Transactions on Industrial Electronics,* vol. 58, no. 1, pp. 85-94, 2011.

[2] T. Hirose and H. Matsuo, "Standalone Hybrid Wind-Solar Power Generation System Applying Dump Power Control Without Dump Load," *IEEE Transactions on Industrial Electronics,* vol. 59, no. 2, pp. 988-997, 2012.

[3] H. Cha, J. Choi, and P. N. Enjeti, "A Three-Phase Current-Fed DC/DC Converter With Active Clamp for Low-DC Renewable Energy Sources," *IEEE Transactions on Power Electronics,* vol. 23, no. 6, pp. 2784-2793, 2008.

[4] Z. Liang, R. Guo, J. Li, and A. Q. Huang, "A High-Efficiency PV Module-Integrated DC/DC Converter for PV Energy Harvest in FREEDM Systems," *IEEE Transactions on Power Electronics,* vol. 26, no. 3, pp. 897-909, 2011.

[5] M. Passalacqua, D. Lanzarotto, M. Repetto, and M. Marchesoni, "Conceptual design upgrade on hybrid pow ertrains resulting from electric improv ements," *International Journal of Transport Development and Integration,* Article vol. 2, no. 2, pp. 146-154, 2018.

[6] G. Su and L. Tang, "A Multiphase, Modular, Bidirectional, Triple-Voltage DC–DC Converter for Hybrid and Fuel Cell Vehicle Power Systems," *IEEE Transactions on Power Electronics,* vol. 23, no. 6, pp. 3035-3046, 2008.

[7] M. B. Camara, H. Gualous, F. Gustin, and A. Berthon, "Design and New Control of DC/DC Converters to Share Energy Between Supercapacitors and Batteries in Hybrid Vehicles," *IEEE Transactions on Vehicular Technology,* vol. 57, no. 5, pp. 2721-2735, 2008.

[8] C. Lai, Y. Cheng, M. Hsieh, and Y. Lin, "Development of a Bidirectional DC/DC Converter With Dual-Battery Energy Storage for Hybrid Electric Vehicle System," *IEEE Transactions on Vehicular Technology,* vol. 67, no. 2, pp. 1036-1052, 2018.

[9] D. Lanzarotto, M. Passalacqua, and M. Repetto, "Energy comparison between different parallel hybrid vehicles architectures," *International Journal of Energy Production and Management,* Article vol. 2, no. 4, pp. 370-380, 2017.

[10] R. Wai, C. Lin, and Y. Chang, "High Step-Up Bidirectional Isolated Converter With Two Input Power Sources," *IEEE Transactions on Industrial Electronics,* vol. 56, no. 7, pp. 2629-2643, 2009.

[11] P. C. Heris, Z. Saadatizadeh, and E. Babaei, "A New Two Input-Single Output High Voltage Gain Converter With Ripple-Free Input Currents and Reduced Voltage on Semiconductors," *IEEE Transactions on Power Electronics,* vol. 34, no. 8, pp. 7693-7702, 2019.

[12] H. Tao, J. L. Duarte, and M. A. M. Hendrix, "Three-Port Triple-Half-Bridge Bidirectional Converter With Zero-Voltage Switching," *IEEE Transactions on Power Electronics,* vol. 23, no. 2, pp. 782-792, 2008.

[13] H. Matsuo, T. Shigemizu, F. Kurokawa, and N. Watanabe, "Characteristics of the multiple-input DC-DC converter," in *Proceedings of IEEE Power Electronics Specialist Conference - PESC '93*, 1993, pp. 115-120.

[14] Z. Qian, O. Abdel-Rahman, and I. Batarseh, "An Integrated Four-Port DC/DC Converter for Renewable Energy Applications," *IEEE Transactions on Power Electronics,* vol. 25, no. 7, pp. 1877-1887, 2010.

[15] G. Chen, Z. Jin, Y. Deng, X. He, and X. Qing, "Principle and Topology Synthesis of Integrated Single-Input Dual-Output and Dual-Input Single-Output DC–DC Converters," *IEEE Transactions on Industrial Electronics,* vol. 65, no. 5, pp. 3815-3825, 2018.

[16] R. Wai, C. Lin, and B. Chen, "High-Efficiency DC–DC Converter With Two Input Power Sources," *IEEE Transactions on Power Electronics,* vol. 27, no. 4, pp. 1862-1875, 2012.

[17] Y. Liu and Y. Chen, "A Systematic Approach to Synthesizing Multi-Input DC–DC Converters," *IEEE Transactions on Power Electronics,* vol. 24, no. 1, pp. 116-127, 2009.

[18] A. Ganjavi, H. Ghoreishy, and A. A. Ahmad, "A Novel Single-Input Dual-Output Three-Level DC–DC Converter," *IEEE Transactions on Industrial Electronics,* vol. 65, no. 10, pp. 8101-8111, 2018.

[19] O. Ray, A. P. Josyula, S. Mishra, and A. Joshi, "Integrated Dual-Output Converter," *IEEE Transactions on Industrial Electronics,* vol. 62, no. 1, pp. 371-382, 2015.

[20] M. Marchesoni and C. Vacca, "New DC–DC Converter for Energy Storage System Interfacing in Fuel Cell Hybrid Electric Vehicles," *IEEE Transactions on Power Electronics,* vol. 22, no. 1, pp. 301-308, 2007.

[21] M. Marchesoni, M. Passalacqua, and L. Vaccaro, "A refined loss evaluation of a three-switch double input DC-DC converter for hybrid vehicle applications," *Energies,* Article vol. 13, no. 1, pp. 1-13, 2020, Art. no. 204.

[22] M. Passalacqua, M. Marchesoni, and L. Vaccaro, "A New Modulation Strategy for Exploiting Discontinuous Conduction Mode in a Double-Input Three-Switch Bidirectional DC-DC Converter," *IEEE Transactions on Industrial Electronics,* vol. 68, no. 11, pp. 10815-10825, 2021.